An Assessment of MJO Circulation Influence on Air–Sea Interactions for Improved Seasonal Rainfall Predictions over East Africa

MARGARET KIMANI

Faculty of Geo-Information Science and Earth Observation, University of Twente, Enschede, Netherlands, and Institute of Meteorological Training and Research, Nairobi,Kenya

JOOST C. B. HOEDJES

Faculty of Geo-Information Science and Earth Observation, University of Twente, Enschede, Netherlands

ZHONGBO SU

Faculty of Geo-Information Science and Earth Observation, University of Twente, Enschede, Netherlands, and School of Environmental Science and Engineering, Chang'an University, Xian, China

(Manuscript received 22 April 2019, in final form 9 July 2020)

ABSTRACT

Rainfall variability affects agriculture planning and water resource management. In extreme flood and drought events, lives and property are destroyed. This study aims to improve East Africa's seasonal rainfall prediction by determining the impact of the standard eight Real-time Multivariate Madden–Julian Oscillation (MJO) (RMM) phases on rainfall and using sea surface temperature (SST) response to test the predictability of the March–May (MAM) and October–December (OND) main rainfall seasons over a period of 33 years (1981–2013). Pearson correlation patterns, composite maps, and regression analyses were applied, and the Brier skill score (BSS) and correlation coefficients (CC) were utilized as validation metrics. Low correspondence of rainfall to MJO 1 and MJO 2 was observed except for the months of November and December. Seasonally, MAM and OND correlation patterns with MJO 2 revealed enhanced rainfall over the highlands and insignificant correspondence over coastal areas. Conversely, enhanced MJO 8 corresponded to suppressed rainfall during the June–August season over the coast and the eastern highlands. MAM rainfall was shown to be predictable using Maritime Continent SST indices, with a BSS of 0.41, while OND rainfall was shown to be predictable using Atlantic and Maritime Continent SSTs with a BSS of 0.62. Positive and negative MJO 2 corresponded, respectively, to enhanced and suppressed rainfall during the OND season and was confirmed to be related to, respectively, a positive and negative Indian Ocean dipole (IOD). An IOD year could possibly be triggered by changes in MJO 2 amplitudes observed as early peaks between February and June.

1. Introduction

Rainfall over East Africa is very variable in space and time and occurs during two main rainfall seasons [i.e., March–May (MAM) and October–December (OND)] in the intertropical convergence zone (ITCZ). Although MAM is the primary rainfall season upon which both water resource management and agricultural planning depend, predicting its variability remains a challenge, with extreme drought and flood events increasing impoverishment and causing economic setbacks. The MAM rainfall season experiences different teleconnections each month (Nicholson 2017). For example, a study by Camberlin and Philippon (2002) has found that spatial rainfall distributions in March and April differ from those in May.

Circulation patterns related to El Niño–Southern Oscillation (ENSO) (Philander et al. 1989) and Indian Ocean dipole (IOD) events (Saji et al. 1999; Webster et al. 1999) have been shown to affect rainfall in East Africa (Indeje et al. 2000; Ogallo 1988). Although these findings have predominantly been linked to OND rainfall, some have been associated with the MAM season

Corresponding author: Margaret Wambui Kimani, m.w.kimani@utwente.nl

DOI: 10.1175/JCLI-D-19-0296.1

(Camberlin and Philippon 2002). The 2010–11 La Niña dry spell affected both the MAM and OND rainfall season, but only the latter was predicted (Lyon and DeWitt 2012). In an earlier study on the influence of La Niña on African rainfall by Nicholson and Selato (2000), a dry spell was observed to be related to warm Indian and Atlantic Oceans. These basins have also been linked to the predictability of ENSO (Frauen and Dommenget 2012). On an interannual time scale, the mean sea level pressure (MSLP) and SST over these basins influence the MAM rainfall onset and cessation over East Africa (Camberlin and Okoola 2003). The cooling and warming over the Indian and South Atlantic Oceans are associated with high and low MSLP anomalies, respectively, which influence enhanced equatorial easterlies and surface divergence over East Africa.

Knowing the dominant source of moisture is essential in understanding rainfall variability. As the ITCZ passes over the equator, a large degree of moisture flux from the Indian Ocean to the Horn of Africa increases rainfall variability (Nicholson 1996). The general position of the ITCZ therefore influences the wetness or dryness over East Africa (Souverijns et al. 2016). According to a study by Nicholson (1996), the ITCZ's movement is regulated by the strength of subtropical highs and the anomalous westerlies. Because the westerlies are associated with MJOs (Pohl and Camberlin 2006a), their interactions are of interest in understanding rainfall variability across the region. MJO is an intraseasonal oscillation with a time scale of 30–60 days; it originates in the Indian Ocean (Matthews 2008), propagating eastward at a speed of 5 m s^{-1} (Madden and Julian 1994). Its circulations may explain intraseasonal weather and climate variations and are associated with convective activity over Africa, similar to the equatorial Rossby and Kelvin waves during monsoons (Matthews 2004). Real-time Multivariate MJO series (RMM1 and RMM2) describe MJO strength and the location of its convective center (Wheeler and Hendon 2004). They are derived from the first two empirical orthogonal functions (EOFs) of combined daily mean fields of outgoing longwave radiation (OLR) and 850- and 200-hPa zonal winds.

Although the relationship of MJO and rainfall over equatorial Africa has been studied (Berhane and Zaitchik 2014; Pohl and Camberlin 2006a; Wilson et al. 2013; Zaitchik 2017), as well as investigated operationally by Omeny et al. (2008), insufficient work has been undertaken regarding the impact of MJO for seasonal rainfall forecasting. This study aims to improve seasonal rainfall predictions over East Africa, by assessing the impact of MJO amplitudes on air–sea interactions (rainfall and SST) using monthly and seasonal time scales over a period of 33 years (1981–2013). Mean low

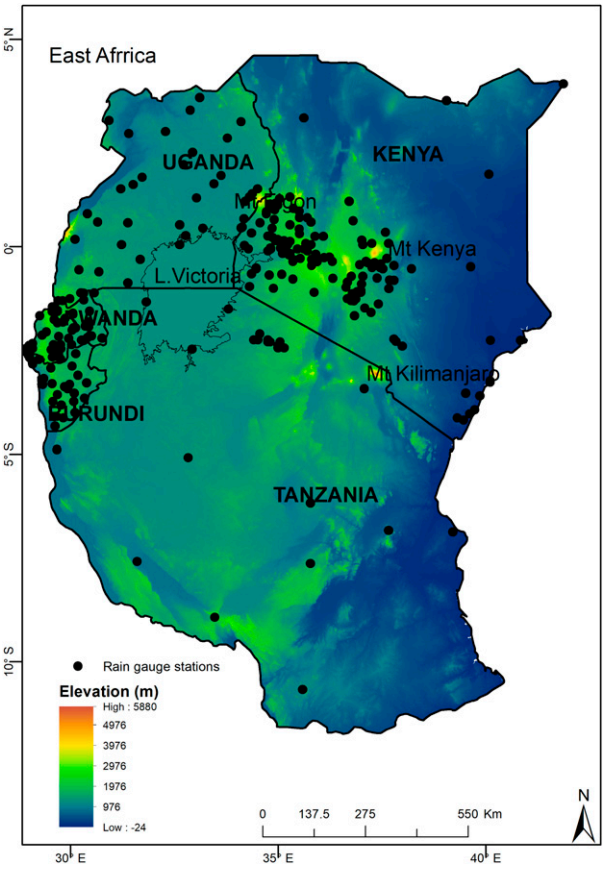

FIG. 1. Map of East Africa depicting elevation variations and rain gauge stations used in gridding and local bias correction of the CHIRPS rainfall data.

level (850 hPa) wind patterns are utilized to qualitatively link ocean dynamics to rainfall variability. An annual stepwise regression prediction model for seasonal rainfall is developed based on the calculated SST indices related to MJOs. Time series and composite maps are employed to establish the MJO link to extreme rainfall events. Section 2 describes the data as well as the methods used for describing RMM's spatial and temporal relationship to rainfall, for the determination of areas with highest variance in SSTs related to MJO forcing, for the development of a regression model of the extracted significant SSTs as seasonal rainfall predictors, and the evaluation of model skill. Section 3 provides the obtained results regarding MJO's relationship to rainfall and SST, spatially and temporally, as well as the regression model output. The discussion and conclusions are presented in section 4.

2. Data and methods

The study area is situated in East Africa between 29° and 42°E and between 12°S and 5°N. The area comprises

five countries: Kenya, Uganda, Tanzania, Burundi, and Rwanda (Fig. 1). To the east, East Africa borders the Indian Ocean, which forms a source of moisture influx. Although there are two primary rainfall seasons, MAM and OND, a third season occurs, primarily over western Kenya and some parts of Uganda, during the southwest monsoon months between June and August (JJA). The latter enhances agricultural production and water resource sectors and is therefore also economically important to the region. In this study, although analysis included all seasons, improved prediction testing was applied to the primary rainfall seasons, as their prediction is most significant to agricultural practices and other applications. The MAM rainfall season experiences different teleconnections each month (Nicholson 2017). For example, spatial rainfall distribution in March and April differs from the May distribution (Camberlin and Philippon 2002). In this study, these differences are explored using monthly and seasonal time scales.

a. Data

Monthly rainfall data were obtained from the CHIRPS v2.0 dataset developed by the U.S. Geological Survey (USGS) Earth Resources Observation and Science Center and the University of California Santa Barbara Climate Hazards Group. In a study assessing satellite rainfall products using ground-based products over East Africa (Kimani et al. 2017), CHIRPS v2.0,TRMM-3B43, and CMORPH v1 displayed the best performance of the seven satellite precipitation products evaluated. However, all products exhibited systematic errors, which were predominantly locally induced and needed to be minimized before the product could be applied. CHIRPS was selected for this study based on its long climatology history, making it suitable for long-term application. To improve CHIRPS' local rainfall representation, a Bayesian correction was applied, using the gridded data from an in situ rain gauge network (Kimani et al. 2018). Further assessment of CHIRPS' performance relative to other products may be found in Toté et al. (2015).

Daily RMM amplitudes (Wheeler and Hendon 2004) were downloaded from the Australian Bureau of Meteorology website (http://www.bom.gov.au/climate/mjo/). The MJO magnitude's impact on East African rainfall was assessed on both a monthly and seasonal scale, from which a seasonal rainfall prediction model was created for the MAM and OND seasons. The impact of MJO phases was assessed based on the sea surface response to MJO forcing. Zonal (U) and meridional (V) wind ($\mathrm{m\,s^{-1}}$) components from ERA-Interim monthly means reanalysis model products (Dee et al. 2011) were used to determine the spatial wind patterns over East Africa monthly and seasonally. The atmospheric winds were all resampled using the nearest neighbor method at 0.05° spatial scale to be compatible with the bias-corrected CHIRPS data.

The terrain across the region is complex, comprising mountains reaching higher than 5000 m above mean sea level, coastal lowlands, and large inland water bodies such as Lake Victoria. An elevation map for East Africa (Fig. 1) was derived from a 90-m-resolution digital elevation model (DEM) downloaded from the Shuttle Radar Topography Mission (SRTM) (Reuter et al. 2007). Using geographical information system (GIS) functionality, 5°-spatial-resolution tiles were mosaiced over the entire region.

b. Methods

1) MJO amplitudes and rainfall indices

Real-time Multivariate MJO series 1 and 2 (RMM 1, RMM 2), as described by Wheeler and Hendon (2004), were utilized to define the various phases and magnitudes of the MJO. The circulation indices characterized convection over eight geographical locations numbered 1 to 8, and representing the Indian Ocean (2, 3), Africa and the Western Hemisphere (1, 8), the Maritime Continent (4, 5), and the Pacific region (6, 7), as described by Wheeler and Hendon (2004). The approximate locations, as described by Donald et al. (2004), were derived from combined empirical orthogonal functions of 850- and 200-hPa zonal winds plus outgoing longwave radiation developed into a pair of principal component time series. The daily magnitude values of RMM were averaged individually every month for each of the eight indices. To characterize the relationship between rainfall and MJO indices, significant correlation coefficients at a 95% confidence level were determined. Similarly, each of the standardized MJO and rainfall indices were correlated monthly and seasonally to obtain a general view of the MJO and rainfall relationships. Z-score (Clark-Carter 2014) standardization was employed for all the variables before comparisons were conducted.

2) Assessment of SST response to MJO forcing

In this section, the average RMM indices and their corresponding magnitudes were compared with SST on a seasonal scale to identify the impact of MJO circulation on the SST. Only MAM and OND seasons were considered for these assessments since they showed significant correlation on a temporal basis. Furthermore, agricultural production and water resource management depended on these main rainfall seasons. To identify suitable SST indices Pearson correlation patterns were used with MJO 1 and MJO 2, as they were

most dominant in the two seasons. After the patterns were visually checked for significant correlation, SST indices were extracted and compared with corresponding annual rainfall indices. Although MJO 1 and 2 showed similar patterns regarding SST, MJO 2 had higher impact than MJO 1 and was therefore used to delineate areas of variance for SST extraction.

3) Prediction of MAM and OND seasonal rainfall

All the variables were standardized using the Z-score index (ZSI) before regression analysis. Only SSTs with temporal significant correlations at 95% confidence level with rainfall were subjected to stepwise regression analysis as predictors of rainfall. Each season of MAM and OND was considered separately.

4) Model performance evaluation

Leave-one-out cross validation was employed to assess the stepwise regression model outputs. The approach was chosen based on the limited data points for climate analysis (33 years). For the probabilistic test, the BSS derived from the BS (Roulston 2007) was used, while correlation coefficients (CCs) were used for the deterministic test. Since the ZSI (Griffiths et al. 1998) and the Standardized Precipitation Index (SPI) are performed in a similar manner (McKee et al. 1993), ZSI was used to determine the probability of the estimated and predicted seasonal rainfall index. The empirical probability of Farahmand and AghaKouchak (2015) was then utilized to derive a nonparametric standardized index [Eq. (1)], instead of using a parametric gamma equation. Moreover, a BS [Eq. (2)] and BS climatology (BS_{clim}) [Eq. (3)] were applied to determine the BSS [Eq. (4)]. Equation (5) describes the Pearson correlation:

$$p(x_i) = \frac{(i - 0.44)}{N + 0.12}, \tag{1}$$

$$\mathrm{BS} = \frac{1}{N}\sum_{j=1}^{N}(f_j - O_j)^2, \tag{2}$$

$$\mathrm{BS}_{\mathrm{clim}} = \overline{o}(1 - \overline{o}), \tag{3}$$

$$\mathrm{BSS} = 1 - \frac{\mathrm{BS}}{\mathrm{BS}_{\mathrm{clim}}}, \tag{4}$$

$$\mathrm{CC} = \frac{\frac{1}{N}\sum_{i=1}^{N}(\mathrm{ob}_j - \overline{\mathrm{ob}})(\mathrm{fc}_i - \overline{\mathrm{fc}})}{\sigma_o \sigma_f}, \tag{5}$$

where i denotes the rank of the nonzero precipitation data, beginning with the smallest, and $\overline{o}$ is the corresponding observed empirical probability, "ob" is the observed rainfall index, and "fc" is the predicted rainfall index. Using this empirical approach, f_j is the predicted probability of the event occurring according to the jth forecast, and o_j is equal to 1 or 0, respectively, depending on whether the event subsequently occurred or not. $\mathrm{BS}_{\mathrm{clim}}$ is the climatological probability, and o (with a bar) is the sample climatology, while N is the period (33 years in this study). The Student's t test was used to test the correlations.

3. Results

a. Comparison of MJO indices and rainfall

This section presents an analysis of the comparison between the eight RMM magnitudes and rainfall on a monthly and seasonal time scale. First, based on the monthly analysis of the averaged daily MJOs for the study period (1981–2013), significant correlations (~0.3) were observed with MJO 1 and MJO 2 in the months November and December of the OND season (Fig. 2a). MJO 1 was situated over Africa and MJO 2 over the western Indian Ocean, which meant their greatest influence on rainfall variability occurred over East Africa. MJO 6 and MJO 7 were located over the Pacific and showed significant correlation during the southeast monsoon from June to August, when East Africa experienced low rainfall in most parts of the region (apart from in western Kenya). Time series of MJO 1 and MJO 2 were further analyzed. The two MJOs were in phase during the months November and December and showed closer correspondence with rainfall in November (Fig. 2b) than in December (Fig. 2c). The month November depicted a peak in the OND rainfall season, suggesting high MJO 1 and MJO 2 magnitudes could correspond to increased rainfall. Correlation maps of MJO 1 and MJO 2 for the months November and December are shown in Fig. 3. Positive correlation patterns show low variance with MJO 1. With MJO 1 positioned over Africa and MJO 2 over the Indian Ocean, it is understandable that the sea surface had a greater influence on the latter. Since the wind patterns were easterly the influence was more to the central and western parts of East Africa. This concurred with high correlations observed over the eastern highlands. The strong winds may have hindered moisture deposit causing the highlands to act as a trap for this moisture. The strong winds related to low-level diffluence could be associated with the southeast monsoon inhibiting moisture influx farther inland (Wei and Bordoni 2016). Studies by Kinuthia and Asnani (1982) as well as Nicholson (2016) have shown that the interaction of Turkana jets with the Kenya highlands enhanced low-level diffluence.

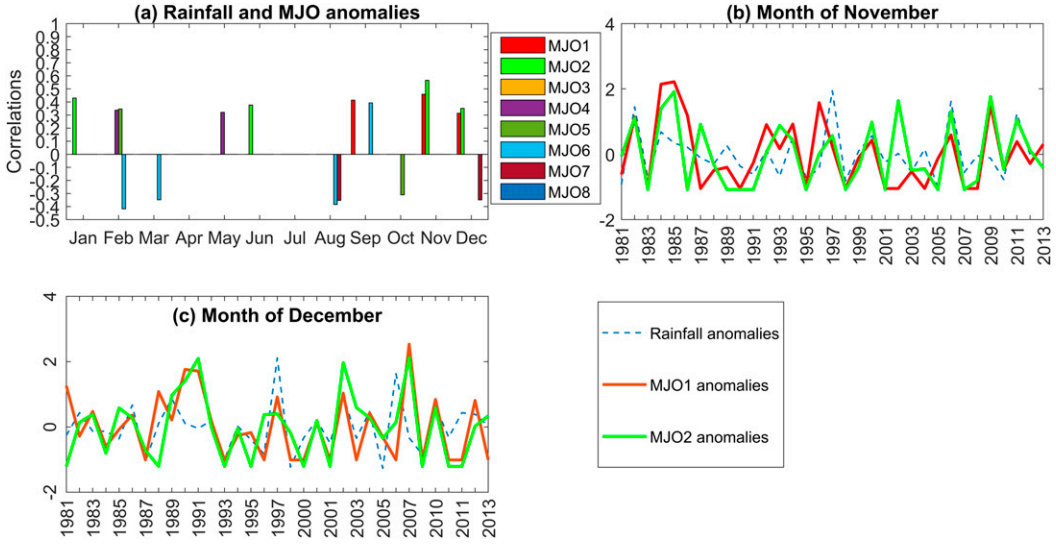

FIG. 2. (a) Monthly correlation coefficients between RMM indices derived from phases 1 to 8 averaged amplitudes and corresponding rainfall. Significant correlations at the 95% confidence level are ≥0.3. Also shown are time series of averaged amplitudes of MJO 1, MJO 2, and corresponding rainfall for the month of (b) November and (c) December.

At seasonal scale, only the dominant MJO phases (MJO2, MJO8) during monthly analysis were utilized. In Fig. 4a the MJO 2 shows a positive correlation with both MAM and OND rainfall seasons. This implies that the enhanced MJO over the Indian Ocean (western part) corresponds to increased main seasonal rainfall over the study region. MJO 8 located over the Western Hemisphere corresponds to suppressed rainfall during JJA (Fig. 4a). The time series for MAM (Fig. 4b) shows more correspondence with MJO 2 than with MJO 1. There are noticeable improvements in correspondence between MJO 1 and MJO 2 and rainfall in the OND season, which concurs with the monthly analysis. Spatial correlation patterns in Fig. 5 show that the dominant phase (MJO 2) corresponded positively with rainfall over the eastern highlands in MAM and OND (Figs. 5a,c, respectively). There is increased correlation during OND that affects mainly the whole of Tanzania (Fig. 5c). Conversely, during JJA (Fig. 5b) negative correlations with MJO 8 are observed, affecting the coastal areas and the eastern highlands. In their study, Pohl and Camberlin (2006b) observed that low-level westerly wind anomalies accompany wet events in the west and easterly wind anomalies those in the east and they associated these opposite impacts with different MJO phases.

b. SST response to MJO 2 forcing

In this section, the SST response to MJO forcing is investigated for the MAM and OND rainfall seasons using correlation patterns within a rectangular area (i.e., 15°S–10°N, 0°–180°E). Only MJO 1 and MJO 2 were utilized as they showed seasonally consistent agreement with rainfall. Figure 6 depicts the MJO 1 and MJO 2 significant correlations with corresponding MAM (Figs. 6a,b) and OND (Figs. 6c,d) SSTs. Similar in both MAM and OND is the cooling over the eastern Atlantic and maritime areas, while over the Pacific warming is observed. However, it is evident that OND has a larger response to MJOs, especially over the maritime areas. Furthermore, OND display positive correlations over the central Indian Ocean that is absent in MAM. This is in line with observations by Wilson et al. (2013) that linked enhanced MJO over eastern Indian Ocean to suppressed East Africa rainfall. To quantify the changes over the oceans, extracted time series (1981–2013) of SST anomalies in rectangular areas were compared to real indexed rainfall over East Africa. Since MJO 2 showed the greatest spatial response in both MAM and OND seasons, MJO 2 was utilized in delineating the areas for SST extraction. In the MAM season, only areas around the Maritime Continent (Fig. 6b) showed significant correlations at 95% confident level, while correlations for the Atlantic proved insignificant. For the OND season both Atlantic and maritime regions were significant with the largest influence (−0.62) occurring over the maritime (Fig. 6d). The extracted SST anomalies for both MAM and OND that had significant temporal correlations with rainfall were then subjected to

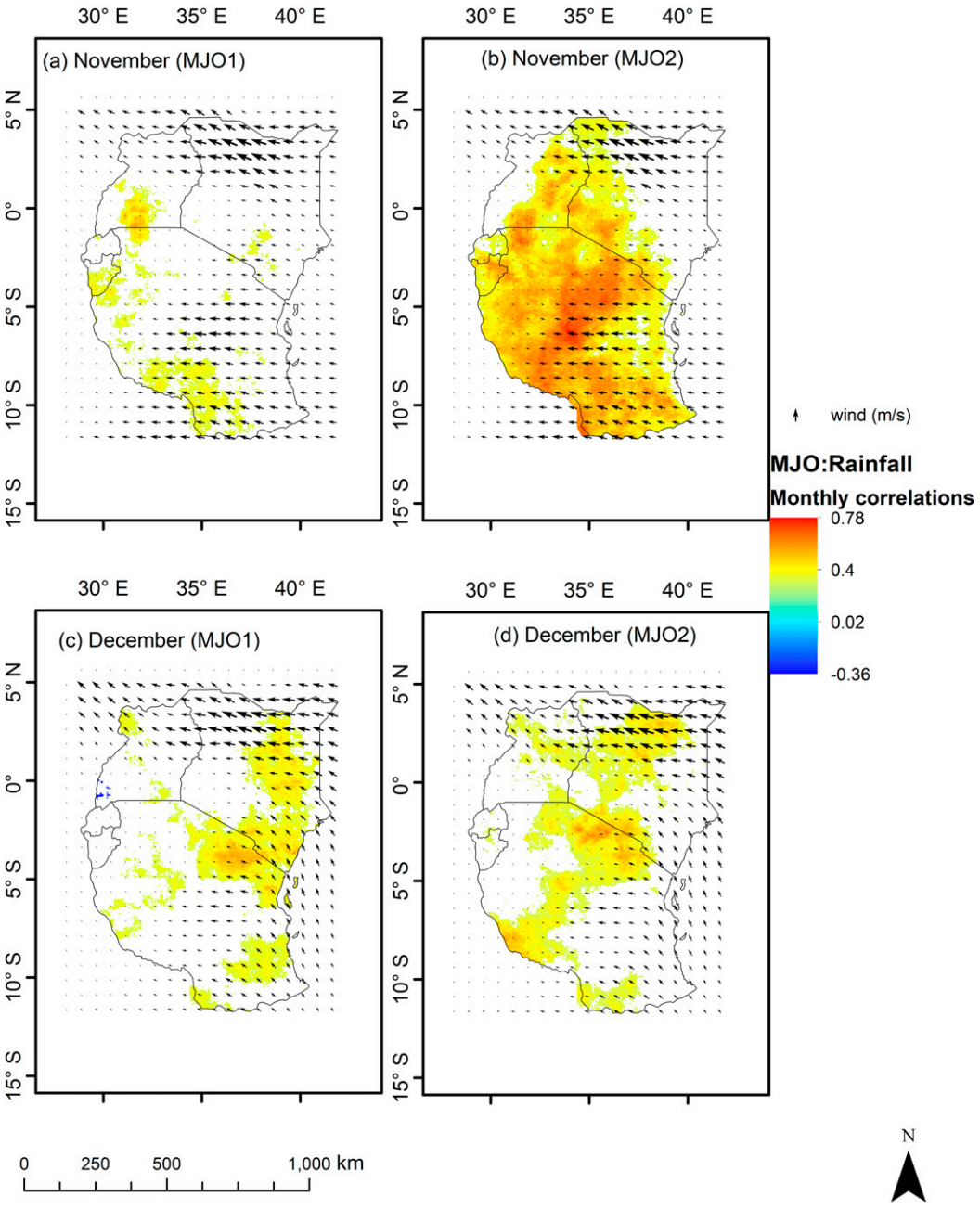

FIG. 3. Monthly correlation coefficients between averaged amplitudes of RMM (a),(c) phase 1 and (b),(d) phase 2 indices and corresponding rainfall. Significant correlations at the 95% confidence level are ~0.3.

regression analysis as predictors of seasonal rainfall on an annual basis.

c. *Seasonal forecasting*

Stepwise regression analysis of the extracted SST indices was designated to predict rainfall index. In performing the regression analysis, leave-one-out cross validation was adopted because of the limited dataset (33 years) for climate prediction. The MAM predictions were not correlated with the estimations (i.e., derived by leave-one-out cross validation); this was attributed to the localized rainfall influence on high elevated areas over the eastern parts of East Africa. Figure 7 shows the time series of the estimated and the predicted rainfall indices. It is evident that there is close correspondence between the estimated and the predicted rainfall during

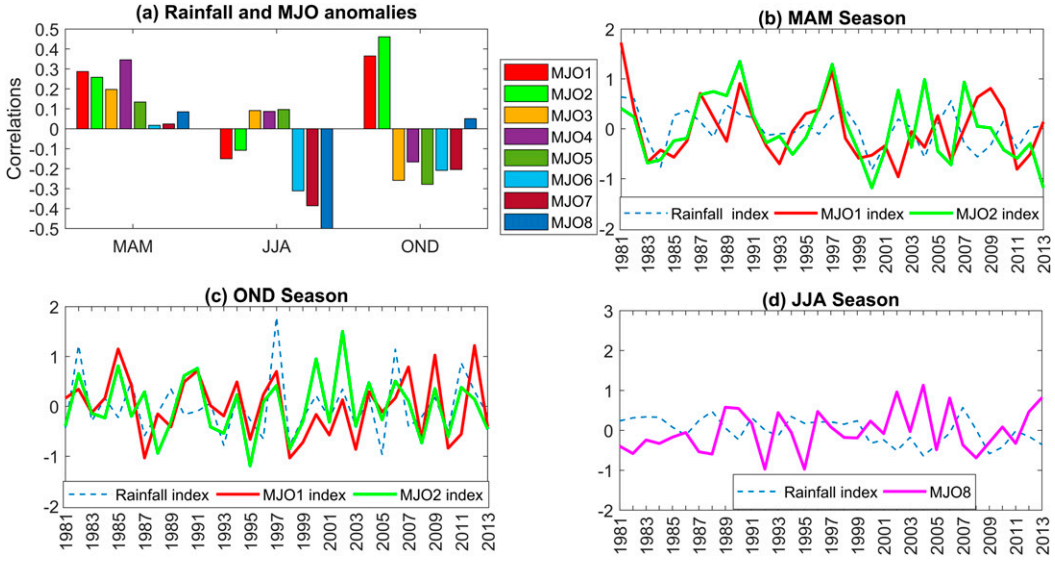

FIG. 4. (a) Seasonal (MAM, JJA, OND) correlation coefficients between RMM indices derived from phases 1 to 8 averaged amplitudes (1981–2013) and corresponding rainfall. Significant correlations at the 95% confidence level are ~0.3. Also shown are time series of averaged seasonal rainfall indices and corresponding amplitudes of MJO 1 and MJO 2 for (b) MAM and (c) OND, and (d) MJO 8 for JJA.

the extreme wet (1982, 1997, 2003, and 2006) and dry (1981, 1984, and 1996) years related to positive and negative IOD (Guo et al. 2015), respectively. Furthermore, observations also show close correspondence for each year prior to the extreme year. MJO modulates ENSO and IOD according to a recent study by Zaitchik (2017). Figure 8 shows the scatter and the residual plots (Figs. 8a,b, respectively). Positive values show closer correspondence than the negative values do (Fig. 8a). This is further supported by residual plots showing large residues toward the negative values (Fig. 8b). The link of MJO 2 to the extreme rainfall events was investigated further using averaged MJO 2 for the OND season. Leave-one-out cross validation was utilized to validate the stepwise regression model of these SSTs as predictors of corresponding seasonal rainfall. Figure 9 shows the plots of MJO 2 for the extreme years of positive and negative MJO 2. During positive MJOs (Fig. 9a), positive indices are clearly defined in the months of OND for the four years, while irregularly high peak (>1) prior positive index is observable between February and June. Similarly, sporadic patterns are observed during negative MJOs (Fig. 9b) except during OND, where negative MJOs appear in one of the months. Seasonal comparisons of those extreme years to corresponding rainfall during the OND season (Figs. 9c,d) indicate that positive and negative MJOs correspond to enhanced and suppressed OND rainfall, respectively. Composite maps of rainfall index during positive (Fig. 10a) and negative (Fig. 10b) MJO 2 support the notion of enhanced and suppressed rainfall, respectively. This leads to the conclusion that MJO circulation enhanced (suppressed) a positive (negative) IOD. Leave-one-out cross validation was utilized to validate the stepwise regression model of these SSTs as predictors of corresponding seasonal rainfall. MAM rainfall was predicted using SST indices related to MJO 2 with a BSS of 0.41, while OND rainfall was predicted with a BSS of 0.62 (Table 1). The low prediction skill in MAM was associated with localized rainfall effects, which resulted in the areal rainfall index insufficiently representing the MJO 2 impact.

Time series of predicted and estimated OND rainfall index indicated close agreement during positive IODs of 1982, 1994, 1997, and 2006 (Guo et al. 2015). Similarly, the dry years (1981, 1984, and 1996) corresponded to negative IODs. This study observed that positive MJOs mainly corresponded with positive IODs of the first type (occurring during the El Niño development phase) of the three types identified by Guo et al. (2015). The negative MJOs corresponded with negative IODs of the second type (following La Niña years) (Guo et al. 2015). Further comparisons of standardized OND MJO 2 amplitudes in relation to corresponding rainfall confirmed positive and negative IODs to be in phase, respectively, with positive and negative rainfall index. The relation of MJO 2 in extreme wet years to IODs was further investigated using OND rainfall composite maps during positive and negative MJO years. Generally, wet and dry conditions over East Africa corresponded, respectively, with positive and negative MJOs years. The

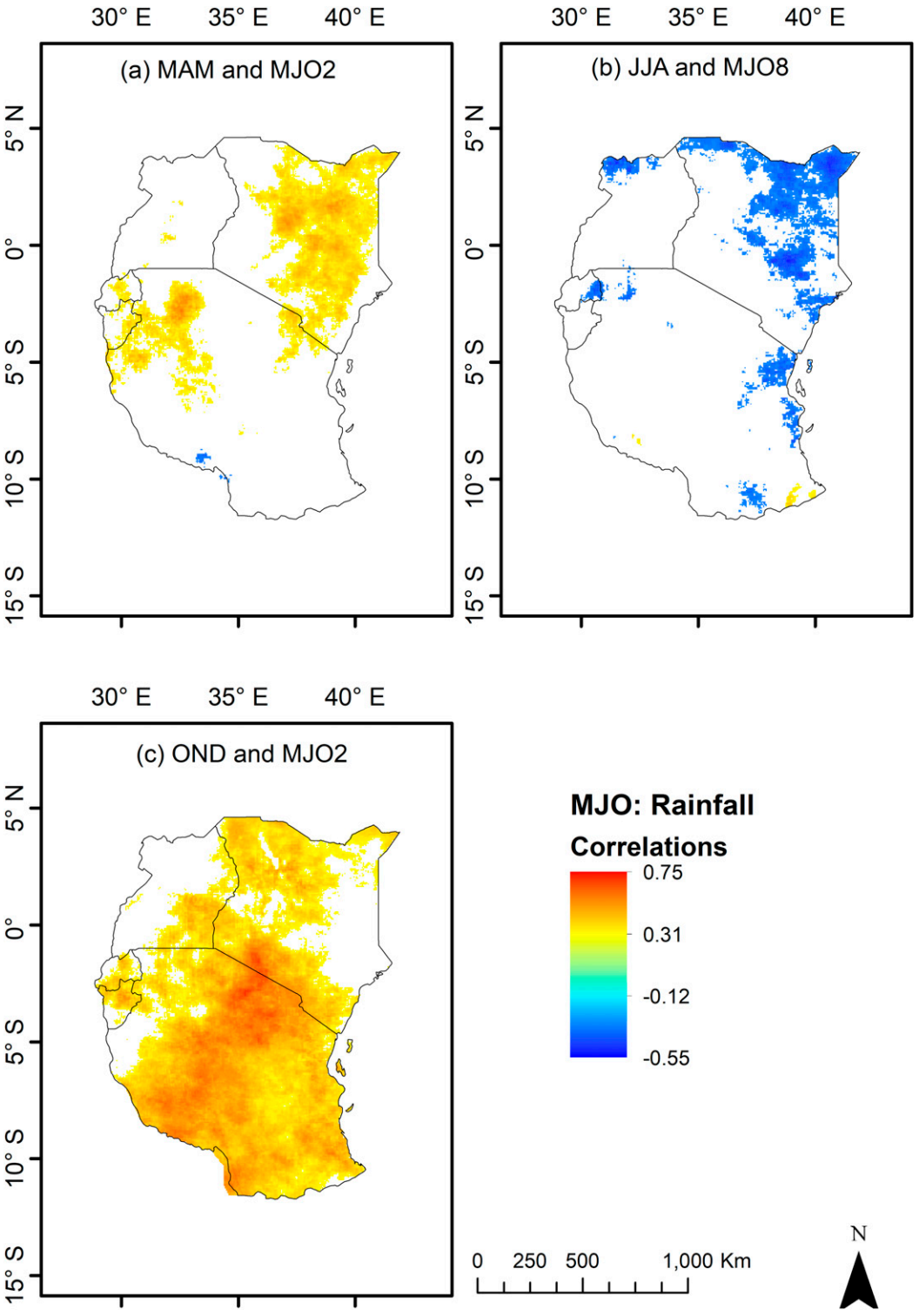

FIG. 5. Seasonal correlation coefficients between RMM (a),(c) phase 2 and (b) phase 8 indices derived averaged amplitudes (1981–2013) and corresponding rainfall. Significant correlations at the 95% confidence level are ~0.3.

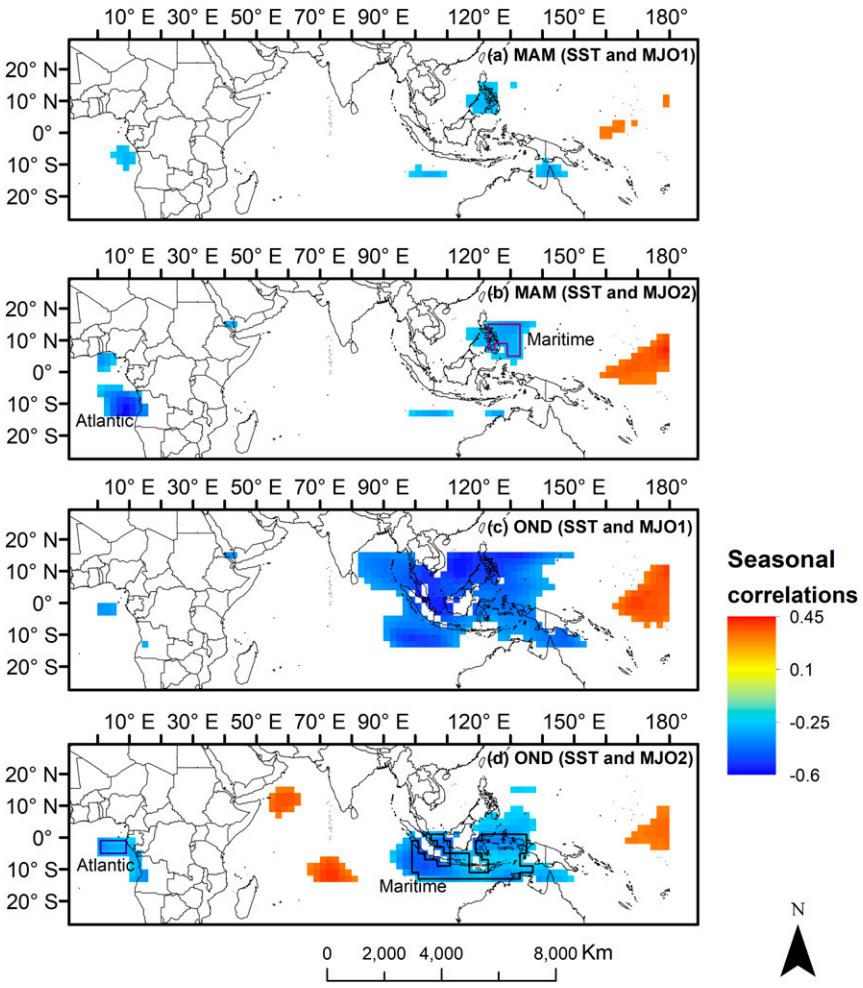

FIG. 6. Sea surface response to RMM phases 1 and 2 as depicted by correlation maps for 33 years (1981–2013). Only significant correlations at the 95% confidence level are shown. For seasonal regression analysis, the sea surface temperature anomalies were extracted from the delineated areas over Atlantic and maritime regions that showed significant temporal correlation with seasonal rainfall indices.

results of these analyses confirmed the impact of MJO 2 on the development and occurrence of IODs.

4. Discussion and conclusions

This study aimed to establish the impact of MJO amplitude on rainfall variability, thereby improving its seasonal prediction over East Africa, based on a period of 33 years (1981–2013). This was achieved in two steps. First, the relationship between the RMM amplitudes (Wheeler and Hendon 2004) and rainfall was determined at monthly and seasonal scale to establish the most influential MJO phase. Second, the identified MJO phase was utilized to ascertain areas of highest SST variance related to its forcing at seasonal scale. Time series of the extracted SST anomalies were compared to an areal standardized rainfall index over East Africa from which significant SSTs were used as rainfall predictors.

The results of monthly analysis showed poor correspondence of rainfall and MJO magnitude for all phases except for MJO 1 and MJO 2 during November and December. As an MJO could last 30–60 days (Matthews 2004), high magnitude in a single month might not reflect a full active phase. Enhanced MJO 1 and MJO 2 during the two wet months November and December suggested increased moisture influx from the Indian Ocean. Further observation indicated that MJO 2 had a greater influence on rainfall variability than MJO 1. With MJO 2 located over the western Indian Ocean and wind flows easterly, it is suggested that MJO 2 enhanced the moisture influx inland. This was further supported by

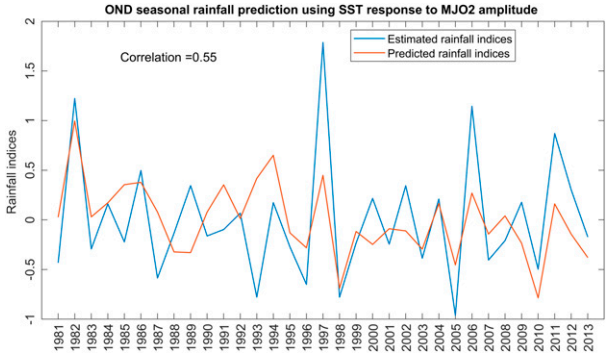

FIG. 7. Time series of October–December (OND) seasonal rainfall indices (estimated and predicted) using SST over the Atlantic and maritime regions related to MJO 2 magnitudes. The predicted values were derived from stepwise regression analysis and leave-one-out cross validation over 33 years (1981–2013).

the correlation maps where MJO 2 showed larger spatial correspondence with rainfall than MJO 1.

This relationship was clearer at seasonal scale as enhanced MJO 1 and MJO 2 significantly corresponded to increased MAM and OND rainfall. A distinct difference in regional dependency of the MJO 1 and 2 influence on rainfall distribution over East Africa was observed. For both seasons, the impact affected highland areas, but during OND large coastal areas showed insignificant correspondence. This is consistent with the observation by Pohl and Camberlin (2006b) that the eastern part of East Africa benefited from moisture influx from the Indian Ocean during the MAM season. MJO 6 and MJO 7 over the Pacific, and MJO 8 of the Western Hemisphere, corresponded to suppressed rainfall during the JJA season affecting mainly coastal areas and eastern highlands bordering the Indian Ocean. In their operational study, Omeny et al. (2008) observed that MJO 2 over the Indian Ocean corresponded to enhanced rainfall over East Africa, while MJO 6 and MJO 7 over the Pacific corresponded to suppressed rainfall. It can be understood that stable conditions prevailed over East Africa during JJA, except in western Kenya that experienced wet conditions. Since MAM and OND formed the two main rainfall seasons over East Africa affecting livelihood and economy, further analysis of the JJA season was left for future research.

MJO 1 and MJO 2 were utilized to identify SST indices responsive to MJO forcing within a rectangular area formed by 15°S–15°N, 0°–180°E. Pearson correlation patterns were analyzed between MAM and OND SSTs and MJO 1 and MJO 2 for a 33-yr period (1981–2013). Enhanced MJO 1 and MJO 2 corresponded to cooling over the eastern Atlantic and maritime areas, and to warming over the Pacific for both seasons. Further observation indicated warming over the western

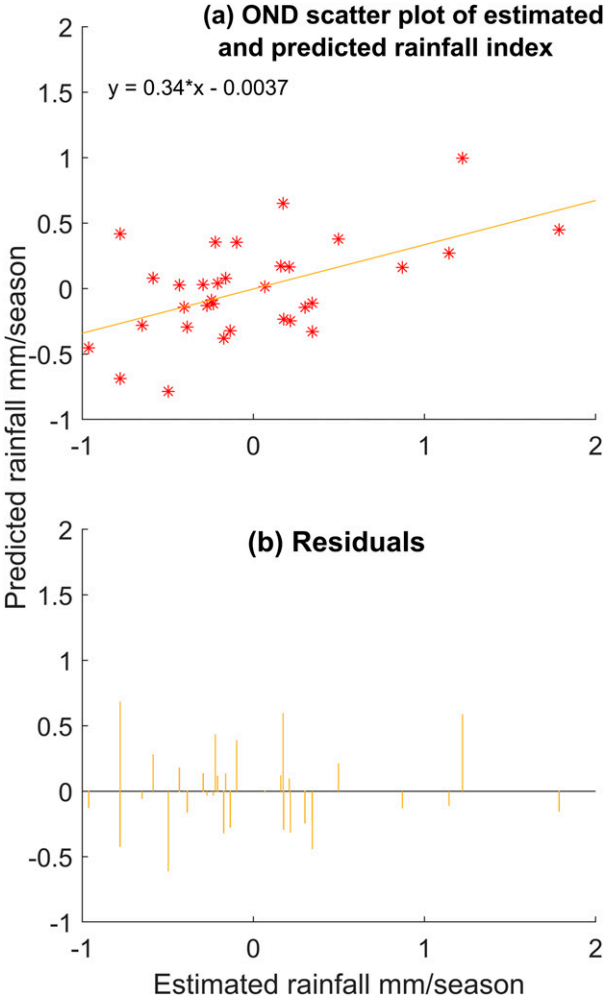

FIG. 8. (a) Scatter and (b) residual plot of October–December (OND) seasonal rainfall index (estimated vs predicted rainfall). Predictions are derived from leave-one-out cross validation of stepwise regression with SST over the Atlantic and maritime regions related to MJO 2 magnitudes as predictors over 33 years (1981–2013).

Indian Ocean related to MJO 2 during the OND season, which was absent during MAM, suggesting a connection to the IOD. The enhanced MJO convection over the eastern Indian Ocean and Maritime Continent was linked to a negative IOD by Wilson et al. (2013) and associated with the suppression of East Africa's rainfall. Similar to analysis with rainfall, MJO 2 depicted more influence on SST in both seasons and was therefore used to delineate areas of highest SST variance.

Time series of standardized SSTs were extracted from these areas and compared to corresponding rainfall over East Africa. Only areas over the maritime significantly corresponded to MAM rainfall, while both the Atlantic and maritime region were significant for OND rainfall.

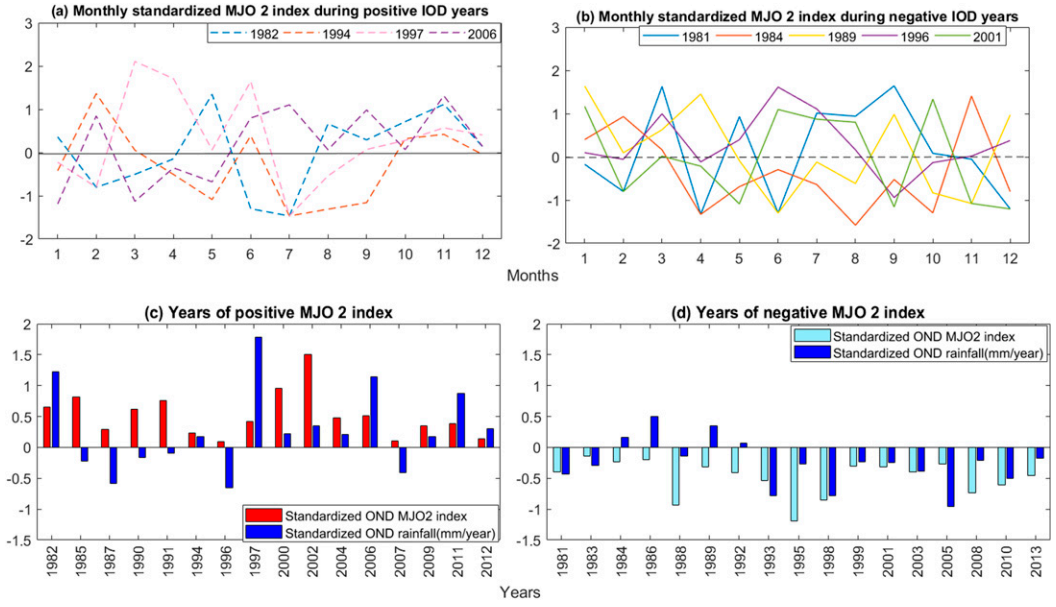

FIG. 9. Monthly plots of standardized MJO 2 index during (a) positive and (b) negative IOD years. Seasonal plots of (c) positive and (d) negative standardized OND MJO2 and corresponding rainfall.

It is worth noting that MAM and OND differed slightly in delineated SST areas, which may be attributed to changes in MJO strength as it progressed eastward with time. Stepwise regression analysis was run using maritime SSTs for MAM, while SSTs of the eastern Atlantic and maritime areas were applied in the OND season as rainfall index predictors. In performing the stepwise regression analysis, the 33-yr study period was

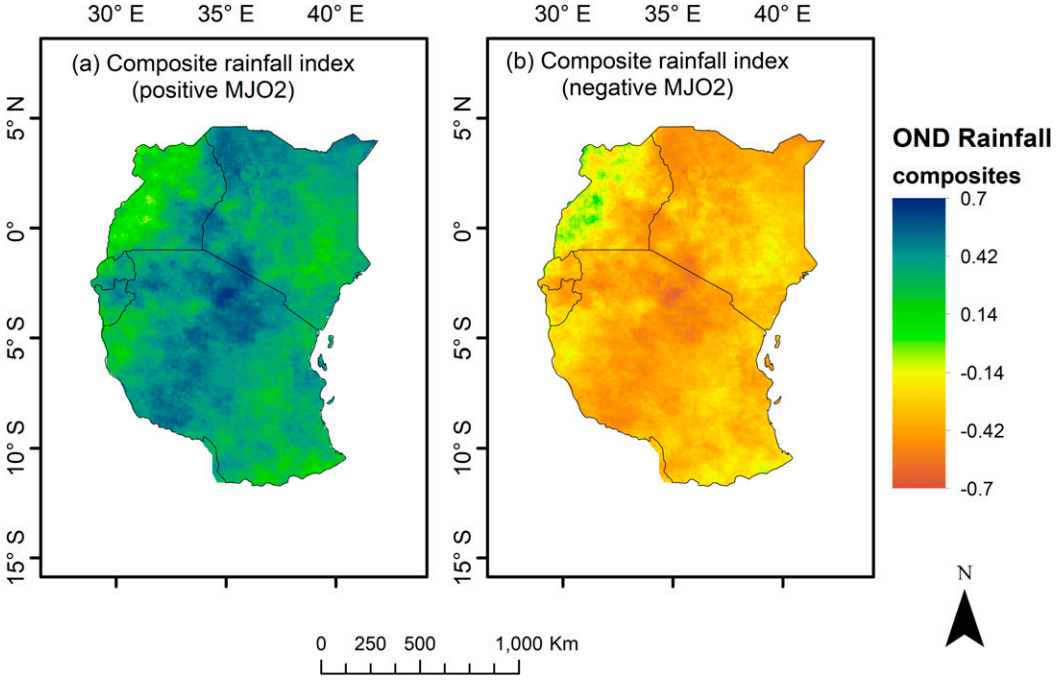

FIG. 10. Composite maps of rainfall index over East Africa during (a) positive and (b) negative MJO 2. The positive MJO 2 years (1982, 1985, 1987, 1990, 1991, 1994, 1996, 1997, 2000, 2002, 2004, 2006, 2007, 2009, 2011, and 2012) included the positive IOD years 1982, 1994, 1997, and 2006. The negative MJO 2 years (1981, 1983, 1984, 1985, 1987, 1988, 1989, 1992, 1993, 1995, 1998, 2001, 2003, 2005, 2008, 2010, and 2013) included the negative IOD years 1981, 1984, 1989, 1998, 2001, 2005, and 2010.

TABLE 1. Regression model prediction output for seasonal (mm per season) indices as predicted by sea surface temperature (SST) indices extracted from the eastern Atlantic and the Maritime Continent as predictors related to MJO 2 forcing during the leave-one-out cross validation period (1981–2013).

Season	BS	BSS	BS_{clim}	CC	SST predictors
MAM	0.17	0.41	0.25	0.03	Maritime Continent
OND	0.09	0.62	0.25	0.55	Eastern Atlantic, Maritime Continent

subjected to leave-one-out cross validation, because of the limited dataset for climate prediction (1981–2013). Using maritime SST indices related to MJO 2, MAM rainfall was predicted with a Brier skill score (BSS) of 0.41. The low prediction skill for MAM was associated with localized rainfall effects resulting in poor representation of the East African areal rainfall index. Time series of estimated and predicted OND rainfall indices indicated close agreement during positive and negative IODs (Guo et al. 2015) related to first type (the development stage, during El Niño years) and second type (following La Niña years) IODs, respectively (Guo et al. 2015). Further, positive and negative IODs were observed to be in phase with positive and negative rainfall indices, respectively. The impact of MJO 2 in extreme wet years was further investigated using OND rainfall composite maps from positive and negative MJO years. Wet and dry conditions over East Africa corresponded to positive and negative MJO years, respectively, confirming the impact of MJO 2 on the development of IODs.

Whereas the influence of MJO on rainfall during MAM was fairly minor, it was concluded that MJO had a major impact on the rainfall dynamics during the OND rainy season. Positive MJO 2 enhanced positive IODs, while negative MJO 2 suppressed negative IODs. Although the signals were observable prior to the OND season as the MJO magnitude reached 1 or more (between February and June), a peak in March and May corresponded to strong IOD events. Consequently, inclusion of the MJO 2 magnitude could help improve seasonal forecasting for the OND rainy season in East Africa.

Acknowledgments. This research is sponsored through funding provided by the Netherlands Fellowship Program (NFP) and by the ITC foundation scholarship program (FSP). No conflict of interest exists. The Digital Elevation Model (DEM) was downloaded from the Shuttle Radar Topography Mission (SRTM). The wind data were acquired from the ERA-Interim data of the European Centre for Medium-Range Weather Forecasts (ECMWF). The CHIRPS v2 dataset was developed by the U.S. Geological Survey (USGS) Earth Resources Observations and Science Centre and the University of California Santa Barbara Climate Hazards Group. The monthly gridded (0.05° × 0.05°) rain gauge data were obtained from the Intergovernmental Authority on Development (IGAD) Climate Prediction and Applications Centre (ICPAC) regional office in Nairobi, through the Kenya Meteorological Department (KMD).

REFERENCES

Berhane, F., and B. Zaitchik, 2014: Modulation of daily precipitation over East Africa by the Madden–Julian oscillation. *J. Climate*, **27**, 6016–6034, https://doi.org/10.1175/JCLI-D-13-00693.1.

Camberlin, P., and N. Philippon, 2002: The East African March–May rainy season: Associated atmospheric dynamics and predictability over the 1968–97 period. *J. Climate*, **15**, 1002–1019, https://doi.org/10.1175/1520-0442(2002)015<1002:TEAMMR>2.0.CO;2.

——, and R. E. Okoola, 2003: The onset and cessation of the "long rains" in eastern Africa and their interannual variability. *Theor. Appl. Climatol.*, **75**, 43–54, https://doi.org/10.1007/s00704-002-0721-5.

Clark-Carter, D., 2014: Z Scores. *Wiley statsRef: Stat. Ref. Online*, https://onlinelibrary.wiley.com/doi/abs/10.1002/9781118445112.stat06236.

Dee, D. P., and Coauthors, 2011: The ERA-Interim reanalysis: Configuration and performance of the data assimilation system. *Quart. J. Roy. Meteor. Soc.*, **137**, 553–597, https://doi.org/10.1002/qj.828.

Donald, A., H. Meinke, B. Power, M. Wheeler, and J. Ribbe, 2004: Forecasting with the Madden-Julian Oscillation and the applications for risk management. *Proc. Fourth Int. Crop Science Congress*, Brisbane, QLD, Australia, Australian Centre for International Agricultural Research, 6 pp., http://www.cropscience.org.au/icsc2004.

Farahmand, A., and A. AghaKouchak, 2015: A generalized framework for deriving nonparametric standardized drought indicators. *Adv. Water Resour.*, **76**, 140–145, https://doi.org/10.1016/j.advwatres.2014.11.012.

Frauen, C., and D. Dommenget, 2012: Influences of the tropical Indian and Atlantic Oceans on the predictability of ENSO. *Geophys. Res. Lett.*, **39**, L02706, https://doi.org/10.1029/2011GL050520.

Griffiths, D., W. D. Stirling, and K. L. Weldon, 1998: *Understanding Data: Principles & Practice of Statistics*. John Wiley & Sons, 401 pp.

Guo, F. Y., Q. Y. Liu, S. Sun, and J. L. Yang, 2015: Three types of Indian Ocean dipoles. *J. Climate*, **28**, 3073–3092, https://doi.org/10.1175/JCLI-D-14-00507.1.

Indeje, M., F. H. M. Semazzi, and L. J. Ogallo, 2000: ENSO signals in East African rainfall seasons. *Int. J. Climatol.*, **20**, 19–46,

https://doi.org/10.1002/(SICI)1097-0088(200001)20:1<19::AID-JOC449>3.0.CO;2-0.

Kimani, M. W., J. C. B. Hoedjes, and Z. B. Su, 2017: An assessment of satellite-derived rainfall products relative to ground observations over east Africa. *Remote Sens.*, **9**, 430, https://doi.org/10.3390/rs9050430.

——, ——, and ——, 2018: Bayesian bias correction of satellite rainfall estimates for climate studies. *Remote Sens.*, **10**, 1074, https://doi.org/10.3390/rs10071074.

Kinuthia, J. H., and G. C. Asnani, 1982: A newly found jet in north Kenya (Turkana channel). *Mon. Wea. Rev.*, **110**, 1722–1728, https://doi.org/10.1175/1520-0493(1982)110<1722:ANFJIN>2.0.CO;2.

Lyon, B., and D. G. DeWitt, 2012: A recent and abrupt decline in the East African long rains. *Geophys. Res. Lett.*, **39**, L02702, https://doi.org/10.1029/2011gl050337.

Madden, R. A., and P. R. Julian, 1994: Observations of the 40–50-day tropical oscillation—A review. *Mon. Wea. Rev.*, **122**, 814–837, https://doi.org/10.1175/1520-0493(1994)122<0814:OOTDTO>2.0.CO;2.

Matthews, A. J., 2004: Intraseasonal variability over tropical Africa during northern summer. *J. Climate*, **17**, 2427–2440, https://doi.org/10.1175/1520-0442(2004)017<2427:IVOTAD>2.0.CO;2.

——, 2008: Primary and successive events in the Madden–Julian Oscillation. *Quart. J. Roy. Meteor. Soc.*, **134**, 439–453, https://doi.org/10.1002/qj.224.

McKee, T. B., N. J. Doesken, and J. Kleist, 1993: The relationship of drought frequency and duration to time scales. *Proc. Eighth Conf. on Applied Climatology*, Boston, MA, Amer. Meteor. Soc., 179–184.

Nicholson, S. E., 1996: A review of climate dynamics and climate variability in Eastern Africa. *Limnology, Climatology and Paleoclimatology of the East African Lakes*, T. C. Johnson and E. O. Odada, Eds., CRC Press, 25–56.

——, 2016: The Turkana low-level jet: Mean climatology and association with regional aridity. *Int. J. Climatol.*, **36**, 2598–2614, https://doi.org/10.1002/joc.4515.

——, 2017: Climate and climatic variability of rainfall over eastern Africa. *Rev. Geophys.*, **55**, 590–635, https://doi.org/10.1002/2016RG000544.

——, and J. C. Selato, 2000: The influence of La Nina on African rainfall. *Int. J. Climatol.*, **20**, 1761–1776, https://doi.org/10.1002/1097-0088(20001130)20:14<1761::AID-JOC580>3.0.CO;2-W.

Ogallo, L. J., 1988: Relationships between seasonal rainfall in east-Africa and the southern oscillation. *J. Climatol.*, **8**, 31–43, https://doi.org/10.1002/joc.3370080104.

Omeny, P. A., L. Ogallo, R. Okoola, H. Hendon, and M. Wheeler, 2008: East African rainfall variability associated with the Madden-Julian Oscillation. *J. Kenya Meteor. Soc.*, **2**, 105–114.

Philander, S. G. H., N. C. Lau, R. C. Pacanowski, and M. J. Nath, 1989: Two different simulations of the Southern Oscillation and El Niño with coupled ocean-atmosphere general circulation models. *Philos. Trans. Roy. Soc. London*, **329A**, 167–178, https://doi.org/10.1098/rsta.1989.0068.

Pohl, B., and P. Camberlin, 2006a: Influence of the Madden-Julian Oscillation on East African rainfall. I: Intraseasonal variability and regional dependency. *Quart. J. Roy. Meteor. Soc.*, **132**, 2521–2539, https://doi.org/10.1256/qj.05.104.

——, and ——, 2006b: Influence of the Madden-Julian Oscillation on East African rainfall: II. March–May season extremes and interannual variability. *Quart. J. Roy. Meteor. Soc.*, **132**, 2541–2558, https://doi.org/10.1256/qj.05.223.

Reuter, H. I., A. Nelson, and A. Jarvis, 2007: An evaluation of void-filling interpolation methods for SRTM data. *Int. J. Geogr. Info. Sci.*, **21**, 983–1008, https://doi.org/10.1080/13658810601169899.

Roulston, M. S., 2007: Performance targets and the Brier score. *Meteor. Appl.*, **14**, 185–194, https://doi.org/10.1002/met.21.

Saji, N. H., B. N. Goswami, P. N. Vinayachandran, and T. Yamagata, 1999: A dipole mode in the tropical Indian Ocean. *Nature*, **401**, 360–363, https://doi.org/10.1038/43854.

Souverijns, N., W. Thiery, M. Demuzere, and N. P. M. Van Lipzig, 2016: Drivers of future changes in East African precipitation. *Environ. Res. Lett.*, **11**, 114011, https://doi.org/10.1088/1748-9326/11/11/114011.

Toté, C., D. Patricio, H. Boogaard, R. van der Wijngaart, E. Tarnavsky, and C. Funk, 2015: Evaluation of satellite rainfall estimates for drought and flood monitoring in Mozambique. *Remote Sens.*, **7**, 1758–1776, https://doi.org/10.3390/rs70201758.

Webster, P. J., A. M. Moore, J. P. Loschnigg, and R. R. Leben, 1999: Coupled ocean-atmosphere dynamics in the Indian Ocean during 1997-98. *Nature*, **401**, 356–360, https://doi.org/10.1038/43848.

Wei, H. H., and S. Bordoni, 2016: On the role of the African topography in the South Asian monsoon. *J. Atmos. Sci.*, **73**, 3197–3212, https://doi.org/10.1175/JAS-D-15-0182.1.

Wheeler, M. C., and H. H. Hendon, 2004: An all-season Real-time Multivariate MJO index: Development of an index for monitoring and prediction. *Mon. Wea. Rev.*, **132**, 1917–1932, https://doi.org/10.1175/1520-0493(2004)132<1917:AARMMI>2.0.CO;2.

Wilson, E. A., A. L. Gordon, and D. Kim, 2013: Observations of the Madden Julian Oscillation during Indian Ocean dipole events. *J. Geophys. Res. Atmos.*, **118**, 2588–2599, https://doi.org/10.1002/JGRD.50241.

Zaitchik, B. F., 2017: Madden-Julian Oscillation impacts on tropical African precipitation. *Atmos. Res.*, **184**, 88–102, https://doi.org/10.1016/j.atmosres.2016.10.002.